Hindawi Publishing Corporation
Journal of Nanomaterials
Volume 2012, Article ID 279810, 11 pages
doi:10.1155/2012/279810

Research Article

Patterning Luminescent Nanocrystalline $LaPO_4$: Eu and $CePO_4$: Tb Particles Embedded in Hybrid Organosilica with Soft-Lithographic Techniques

Sajid U. Khan[1,2] and Johan E. ten Elshof[2]

[1] *Faculty of Materials Science and Engineering, Institute of Space Technology, P.O. Box 2750, Islamabad 44000, Pakistan*
[2] *MESA+ Institute for Nanotechnology, University of Twente, P.O. Box 217, 7500 AE Enschede, The Netherlands*

Correspondence should be addressed to Sajid U. Khan, sajid.ullah@ist.edu.pk

Received 29 September 2011; Revised 3 November 2011; Accepted 3 November 2011

Academic Editor: Shanfeng Wang

Eu^{3+}-doped $LaPO_4$ and Tb^{3+}-doped $CePO_4$ luminescent nanoparticles embedded in hybrid organosilica were patterned by two soft lithographic techniques. The role of various parameters such as solution chemistry, thermal protocols, and modification of the mold-substrate surface energies related to pattern shape formation and adhesion to the substrates have been studied. The shrinkage of the oxide patterns and shape evolution during the process was also examined. The patterns were characterized with optical and photoluminescence (PL) microscopy, X-ray diffraction (XRD), and scanning electron microscopy (SEM). Compositional analyses were carried out with X-ray photoelectron spectroscopy (XPS), low-energy ion scattering (LEIS), and secondary ion mass spectroscopy (SIMS). The results indicated that the final patterns obtained with these two techniques for the same material have different shapes and adherence to the substrates.

1. Introduction

Oxide materials doped with lanthanide ions comprise a class of materials that have great technological importance in areas such as phosphor lamps, displays, sensors, lasers, and optical amplifiers [1–3]. At nanometer scale, these materials have high surface-to-volume ratio and enhanced structural, electronic, and optical properties in comparison to the bulk phase. Generally, oxide materials are known to be good hosts for lanthanide ions, since they provide good quantum yields. For example, lanthanum orthophosphate ($LaPO_4$) is an excellent host for ions such as europium, cerium, and terbium in the fabrication of photoluminescent materials [3, 4].

At present, the most common technologies used for the deposition of these materials are electrophoretic deposition [5–7], screen printing [8], pulsed laser deposition [9, 10], and traditional photolithography [11]. In fact, the patterning techniques used for phosphor screens are known to have a great effect on the resolution of flat panel displays [12].

Soft-lithographic techniques [13] could be used as alternative techniques, when simplicity, ease of use, and cost effectiveness is targeted. They are cheap, easy, and simple and most importantly, they need no clean room conditions or complicated and lengthy processing steps. So far, relatively little work has been reported on the use of soft-lithographic techniques for the patterning of luminescent materials. Yu et al. applied micromoulding in capillaries (MIMIC) to pattern a Pechini sol-gel-based nanocrystalline YVO_4 : A (A = Eu^{3+}, Dy^{3+}, Sm^{3+}, Er^{3+}) phosphor films [12]. Pisignano et al. employed mechanical lithographic techniques to print 1D patterns of light emitting materials embedded in organic films [14]. They reported that patterned films exhibited enhanced luminescence (by more than a factor of two) as compared to nonpatterned films. Similarly, Han and coworkers [15] applied the technique of MIMIC to sol-gel-based phosphor patterned lines having various line widths. The patterned and nonpatterned films exhibited the same optical properties.

Here we report the use of two soft-lithographic techniques, namely, MIMIC [13, 16] and microtransfer moulding (μTM) [13, 17] for the patterning of two types of

luminescent nanoparticles. A comparison between the two techniques has been made based on the degree of filling of the channels, adhesion of the patterned films to the substrate, their shape profiles, and shrinkage behavior. This paper will focus on two important fundamental questions (a) what will be the outcome of applying two different soft-lithographic techniques to one material? (b) What will be the result of patterning two different materials with one technique? This paper will make a great contribution and a step forward towards selecting an appropriate soft-lithographic technique for the right material and applications.

2. Experimental

2.1. Materials. Unless otherwise stated, reagents were used as received without further purification. The organosilane precursor 1,2-bis(triethoxysilyl)ethane (99.999%) abbreviated as BTESE, nitric acid (65%), polyoxyethylene 20 cetyl ether (Brij 58), and ethanol (99.8%) were all purchased from Aldrich. N, N-dimethylformamide (99.8%) (DMF) was purchased from Merck.

2.2. Synthesis of Luminescent Lanthanide Phosphate Nanoparticles. Two types of luminescent nanoparticles (NPs), namely, $LaPO_4$: Eu and $CePO_4$: Tb, having particle diameters (Φ) of 5–8 nm, were used for patterning in the present work. The synthesis route adopted was according to Riwotzki et al. and was scaled down to 10 mmol and slightly modified as follows [18]. To a solution of lanthanide chloride hydrate salts (10 mmol) in methanol (50 mL), tris(2-ethylhexyl) phosphate (TEHP, 60 mL) was added. Under reduced pressure (10 mbar at 60°C), methanol and water were evaporated. Depending on the lanthanide ions used for the synthesis, the remaining solution sometimes remained slightly colored.

In parallel, a solution of crystalline phosphoric acid (980 mg, 10 mmol) in tris(2-ethylhexyl) phosphate (30 mL) and tri-*n*-octylamine (TOA, 13.1 mL, 30 mmol) was prepared. The dissolved acid solution was heated to 80°C, and water and oxygen were removed in the vacuum. The solution was flushed with argon three times before the lanthanide-ion solution was added. Again, the flask was evacuated and flushed with argon three times before the mixture was heated to 200°C for 20 h in order to minimize the oxidation of cerium(III) to cerium(IV). During the reaction, the temperature decreased by 30° to 170–175°C. The heating was stopped at this point, and the colloidal solution was cooled to room temperature. Then, the solution was added to methanol (400 mL) in a separating funnel to precipitate the nanocrystals as a white solid. The nanocrystals were separated from the solution into centrifuge tubes. After centrifuging down the nanocrystals at 1500 g for 5 min, they were suspended in methanol and centrifuged again. This step was repeated three times. The nanocrystals were transferred into a flask and dried with a rotary evaporator yielding a white to yellowish powder (average yield 7.2 mmol, 72%), depending on the composition of the nanocrystals.

2.2.1. Preparation of Nanoparticles Solution Embedded in Hybrid Silica

Solution (a). 10 mg of the $LaPO_4$: Eu NPs were dissolved in 5 mL of DMF and stirred at 100°C for 1 h. In case of $CePO_4$: Tb, the NPs were dissolved in ethanol and stirred for 1 h at room temperature. When needed, the amount of solvent was varied for the adjustment of viscosity.

Solution (b). Aqueous nitric acid (0.5 mL concentrated HNO_3 in 1.8 mL of water) was added dropwise to 1.8 mL of 1,2-bis(triethoxysilyl)ethane (BTESE), and 5.0 mL of ethanol while stirring in an ice bath. The mixture was refluxed for 2-3 h at 60°C.

Solutions of various concentrations were made by mixing solutions (a) and (b) in various proportions. The viscosity was adjusted by adding small amounts of Brij 58 to the final solution and stirring for 2-3 h. The viscosity of the final solution was measured to be 4.210 mPa·s.

3. Results and Discussion

3.1. Patterning of $LaPO_4$: Eu by Micromoulding in Capillaries (MIMIC). Micromoulding in capillaries (MIMIC) technique was applied to pattern $LaPO_4$: Eu nanoparticles (NPs) embedded in hybrid silica. First of all, the Si substrates were cleaned with a fine jet of CO_2 crystals to blow away the dust particles. Then both substrates and PDMS moulds were treated with oxygen plasma (Harrick Plasma, 200 W) at a pressure of 80 Pa using molecular oxygen [19]. Figure 1 shows SEM and AFM images of line- and pit-patterned films. The complete filling of the capillaries took 10–15 min. The wet patterns were then left for 10–60 min. (with the mould) at 80°C on a hot plate in order to evaporate the solvents and were annealed at 300°C for 30 min in nitrogen. Figure 1(a) shows an example of such a line pattern having a line width (w_l) of 6 μm and spacing between the lines (s_l) of 12 μm. The adhesion of the filled mould to the substrate after drying was found to be stronger. In some cases, the strong adhesion resulted in detachment of a residue layer from the mould and stayed on the substrate. An example is shown in Figure 1(b), where the darkest lines, which are mostly located in the lower part of the picture, are the residue lines of PDMS, while the less dark lines between the PDMS residues are actual patterned organosilica lines obtained from a mould having both w_l and s_l of 1.5 μm, respectively. The resulting shapes of the organosilica pattern are not perfect replicas of the PDMS master from which they are obtained, as can be seen in Figure 1(c), having similar dimensions as in Figure 1(b). The patterned lines have a single peak unlike the double-peak profile as reported somewhere else [20]. Figure 1(d) shows an AFM image showing line pattern of the same dimensions as shown in Figures 1(b) and 1(c) and illustrates the surface roughness between the patterned features due to PDMS residues.

The strong adhesion between mould, pattern, and substrate can have two consequences. It may either result in the detachment of PDMS from the mould and its adhesion to the substrate (Figure 1(b)) or in the detachment of

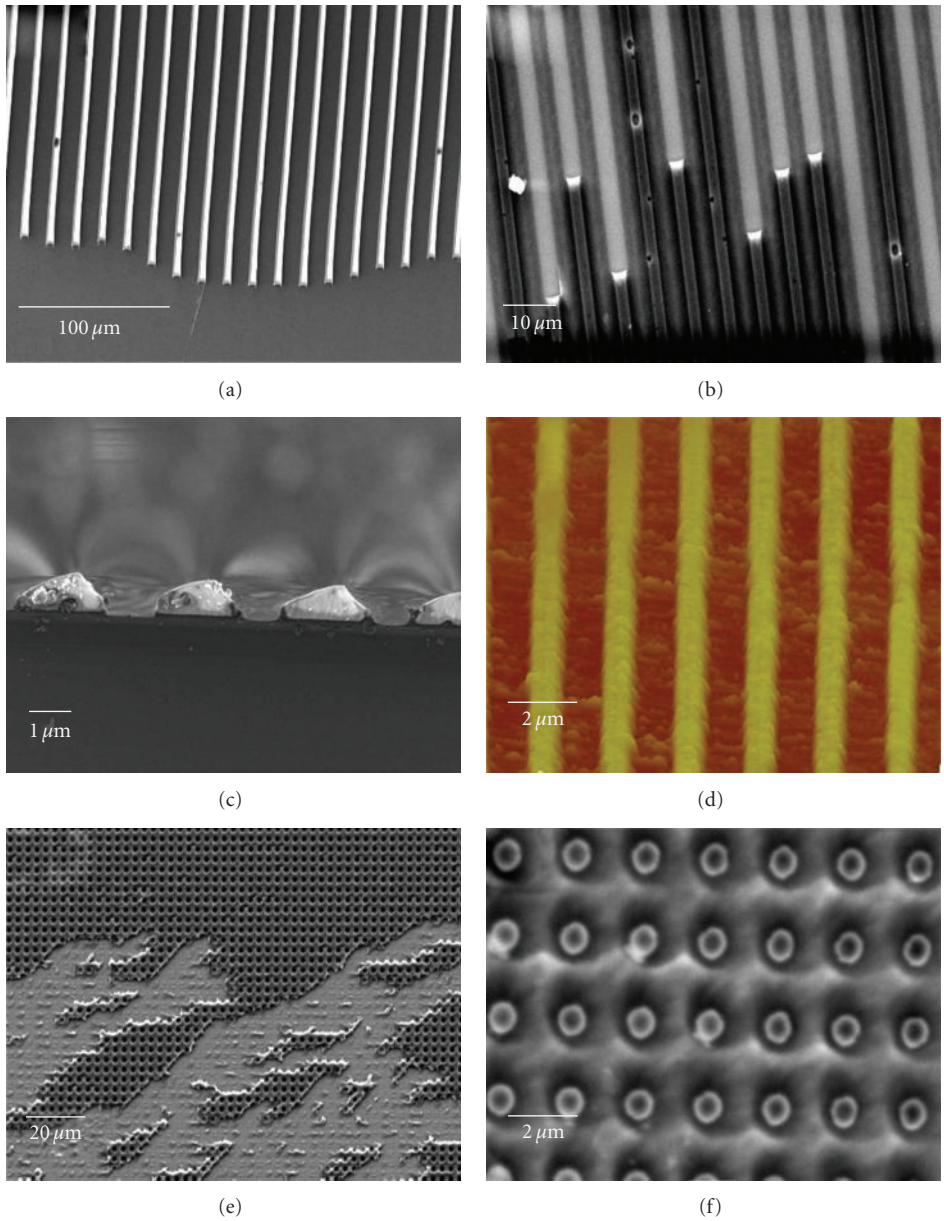

FIGURE 1: SEM and AFM images of $LaPO_4$: Eu NPs embedded in hybrid organosilica and made with the MIMIC technique. (a) SEM image of line patterns having $w_l = 6\,\mu$m and $s_l = 12\,\mu$m; (b) SEM image of a nonannealed line pattern showing patterned lines and PDMS residue having $w_l = 1.5\,\mu$m and $s_l = 1.5\,\mu$m; (c) Cross-sectional SEM image of 1.5 μm patterned lines; (d) AFM image of 1.5 μm wide lines showing surface roughness due to residual PDMS layer; (e) SEM image of pit-patterned film having $P_d = 800$ nm, depicting the detachment of the pattern due to strong adhesion of the film to the mould; (f) pit pattern showing white PDMS residues inside the pit pattern. Here w_l, s_l, and P_d mean the width of the lines, spacing between the lines, and diameter of the pit, respectively.

the patterned film from the substrate. An example of the latter effect is shown in Figure 1(e), where a pit-patterned film having pit diameter P_d of 800 nm was removed together with the mould. This problem can be solved by careful adjustment of the surface energy of the mould by varying the time of plasma treatment, as shown elsewhere [19]. The white areas inside the holes in the pit-patterned film in Figure 1(f) also show the residue layer.

3.2. Patterning of $LaPO_4$: Eu by Microtransfer Moulding. As discussed in the previous section, the adhesion of MIMIC-derived patterned films was too strong that it resulted in the partial detachment (removal) of the patterned material. In order to circumvent this problem we applied microtransfer moulding (μTM). A tiny drop of solution containing NPs was gently placed on a PDMS mould after it had been treated with oxygen plasma for 20–60 s. After removing the excess material from the protruding parts of the mould with a clean PDMS or steel block, the mould was placed and pressed carefully onto a clean Si substrate. Mould and pattern were then placed on a hot plate at 80°C for 10–30 min to solidify the wet pattern. Figures 2(a) and 2(b)

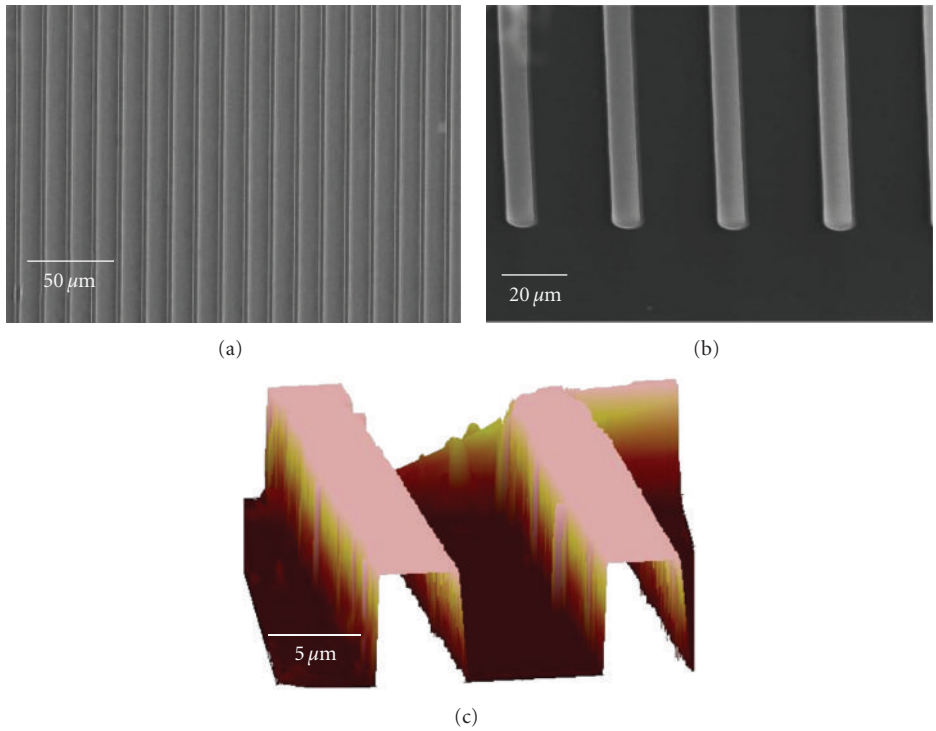

Figure 2: Images of $LaPO_4$: Eu lines having $w_l = 6\,\mu$m and $s_l = 12\,\mu$m patterned with μTM; (a) and (b) SEM images; (c) topographic AFM. The shape of the line is more rectangular than those derived from MIMIC.

show line patterns having w_l and s_l of 6 μm and 12 μm, respectively, and obtained with μTM. Similarly, Figure 2(c) shows an AFM height image of the shape of the pattern. The shape profile is more rectangular than those derived from MIMIC.

The main reason that the shape of the pattern is replicated well with μTM is probably that the channels of the mould are filled prior to replication and exposed to air, to which solvents can evaporate faster and more homogeneously than through the mould as in MIMIC. In μTM the channels are filled with a block unlike MIMIC, where they are filled by capillary action. In other words, the filling phenomenon in MIMIC is rather a spontaneous process whereas in μTM it is a mechanical process.

3.3. Patterning of $CePO_4$: Tb Nanoparticles (NPs). MIMIC and μTM were also applied to pattern $CePO_4$: Tb NPs of various dimensions and shapes. These NPs were stabilized in solvent ethanol unlike $LaPO_4$: Eu NPs which were stabilized in DMF. Figure 3(a) shows a MIMIC-made line-patterned film having w_l of 6 μm. The filling length of the channels was higher, and the evaporation was comparatively faster than that of $LaPO_4$: Eu NPs, which were stabilized in DMF, since ethanol evaporates faster than DMF does. Furthermore, DMF was observed to be less compatible with PDMS, since it is a strong solvent. It degraded the PDMS mold when left in contact for longer periods of time. Figure 3(b) shows a μTM-derived line-patterned film having w_l 3 μm before annealing. Residue PDMS lines between the actual patterned lines can be observed. This was found to happen when the PDMS mould was treated in oxygen plasma for more than 30 s. Longer plasma treatment times increase the surface energy of the mould by oxidizing PDMS to amorphous SiO_x, which is brittle. The surface energy increased the bonding strength between mould and substrate, and the brittleness of the oxidized PDMS layer.

Moulds treated within oxygen plasma for shorter periods of 20–30 s were found to be suitable for replication of features (Figure 3(c)). On the other hand, a mould treated with plasma for a too short period of time reduces the adhesion of the patterned material with the substrate. In that case, the patterned material may detach from the substrate. An example is shown in Figure 3(d), where the displacement of line patterns and their detachment from the substrate can be observed.

An advantage of μTM over MIMIC is the possibility of patterning isolated features. Examples of patterned isolated pillars having diameters (P_d) of 800 and 1500 nm are shown in the lower and upper part of Figure 3(e), respectively. In Figure 3(f), the residue layer between the patterned features is visible. This occurs when the excess solution was not completely removed from the mould prior to their registration onto the substrate.

3.4. Important Aspects of Microtransfer Moulding. Although μTM has some advantages over MIMIC, the adhesion of μTM-made patterned features to the substrate is weaker than that of MIMIC. When patterning line structures, the excess solution should be removed at right angle to the lines. Otherwise, it may cause the removal of the solution from

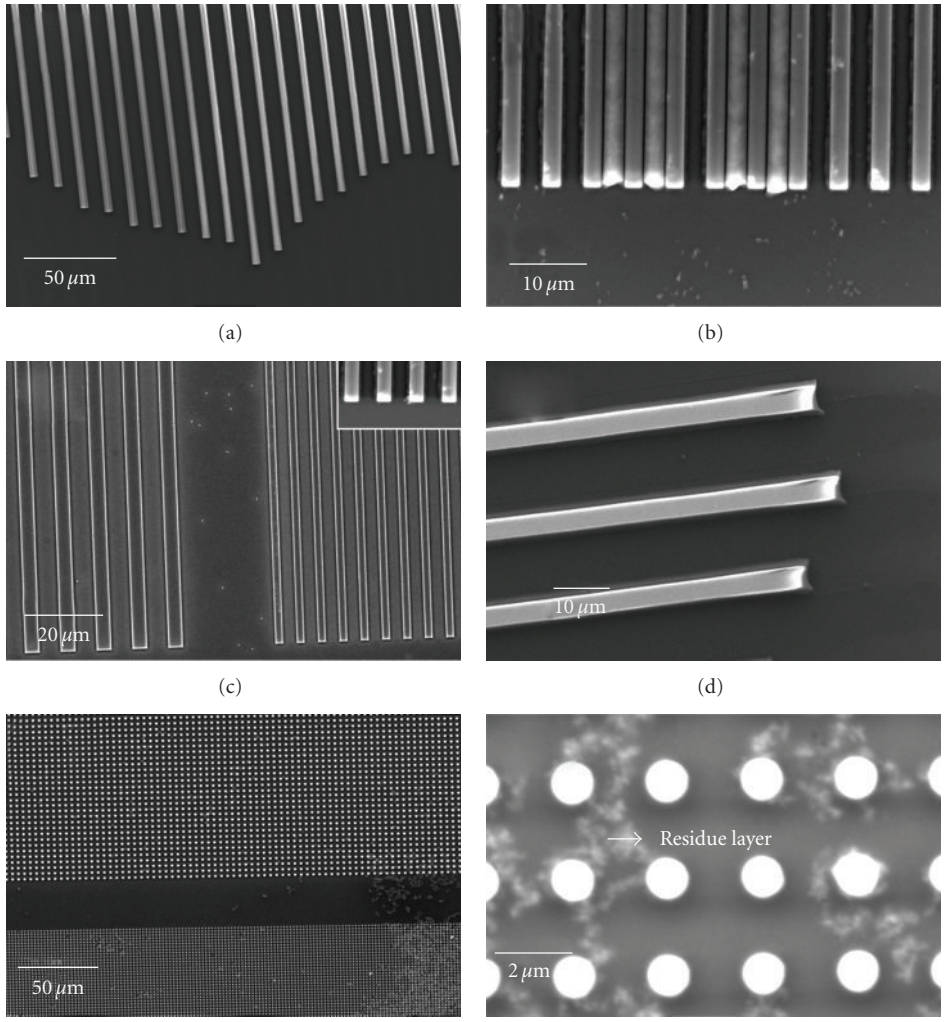

FIGURE 3: SEM images of $CePO_4$: Tb fluorescence NPs in hybrid silica; (a) line pattern made with MIMIC having $w_l = 6\,\mu$m; (b) line pattern made with μTM showing residue of PDMS lines between the patterned lines as a result of strong adhesion; (c) line pattern made with μTM having $w_l = 5\,\mu$m (left) and $w_l = 3\,\mu$m (right); (d) μTM-derived line pattern showing displacement and detachment of the lines due to poor adhesion to the substrate; (e) μTM-derived pillars pattern having diameter of $P_d = 800$ nm (lower part), and $P_d = 1500$ nm (upper part); (f) pillar pattern showing the residue layer between the pillars.

the lines and results in the formation of partially filled M-shaped lines. See Figure 4(a).

The force exerted on a cleaning block to remove excess solution from the mould is also of importance. Application of too large force can cause the partial or complete removal of solution from the patterned area and may lead to incomplete pattern replication. An example is shown in Figure 4(b) (left), where the broken lines resulted from too large forces on the mould. The force applied with a hard material such as steel should be smaller when a soft material is used, such as PDMS. Finally, the excess materials should be removed thoroughly from the mould, or it will be transferred to the substrate and may affect the pattern (Figure 4(c)). All line patterns shown in Figure 4 have w_l and s_l of 6 μm and 12 μm, respectively, and were obtained from a solution of $LaPO_4$: Eu nanoparticles embedded in hybrid silica.

3.5. D Layer-by-Layer Type Patterning. Both techniques can also be applied to produce 3D layer-by-layer type patterns. As discussed in the introduction part that these 3D wood pile patterns may find application in photonics for wave-guiding and photonic crystals. Figure 5 depicts the step-by-step schematic procedure adopted for patterning these 3D structures. The first layer can be patterned with the conventional MIMIC or μTM method (Figure 5(a)). The pattern is then dried at some elevated temperature. After drying, a thin film of some degradable polymer is spin coated on top (Figure 5(b)). In the present work, we applied a thin film of commercially available UV-curable polyurethane (PU) with a speed of 1500 rpm for a period of 1 min. The PU film was cured by exposure to UV light with a wavelength of 350 nm for 2 h. Subsequently, the PU film was treated in oxygen plasma for 5–10 min in order to improve its adhesion

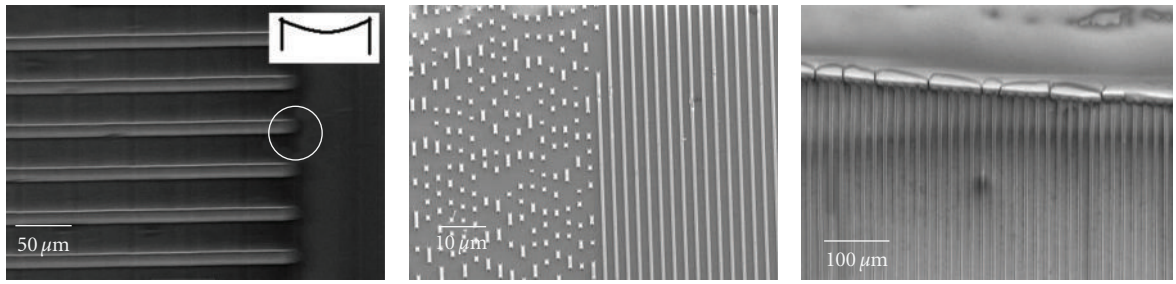

Figure 4: SEM images showing the effects of various processing variables in μTM (a) removal of the excess material in a direction parallel to the lines results in M-shaped lines; (b) application of strong force during the removal of excess material may result in incomplete filling of features of the mould; (c) reservoir (bulk) of excess material at the edge of the patterned lines resulting from incomplete removal of excess solution.

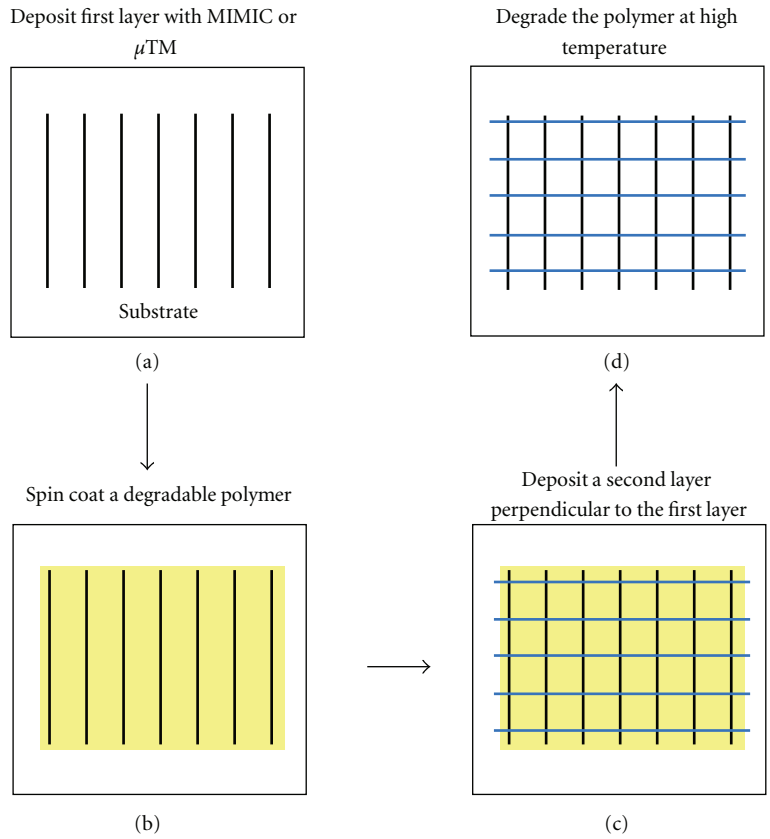

Figure 5: Schematic illustration of the procedure adopted for 3D wood pile pattern fabrication.

to the PDMS mould for the next layer to be deposited. A fresh PDMS mould was also treated in oxygen plasma for 5 min and placed very carefully on top of the PU film in such a way that channels of the mould were oriented perpendicular to the lines of the first layer. Then a second layer was patterned on top of the PU film (Figure 5(c)). Finally, after drying, the buried PU film can be degraded by annealing the sample at 550°C in air for 2 h. This yielded a 3D wood pile pattern (Figure 5(d)).

In principle, the same procedure is expected to be applicable to stack a third or more layers. However, defects and errors that occur in one layer will be transmitted to the layers above. Thus, increasing the number of layers also promotes the number of defects in the final pattern, especially in the upper layers. Furthermore, the weight of the mould while placing it on top of the green body may also produce defects. It was found that the adhesion of the second layer to the underlying PU/titania substrate was weaker than the adhesion of the first layer to the substrate. The adhesion was improved by oxygen plasma treatment of the polymer film for 5 min prior to deposition of the second layer.

While the MIMIC-derived patterns showed good adhesion to the substrate, the final line shapes were not perfectly rectangular; this is an undesirable feature when 3D type

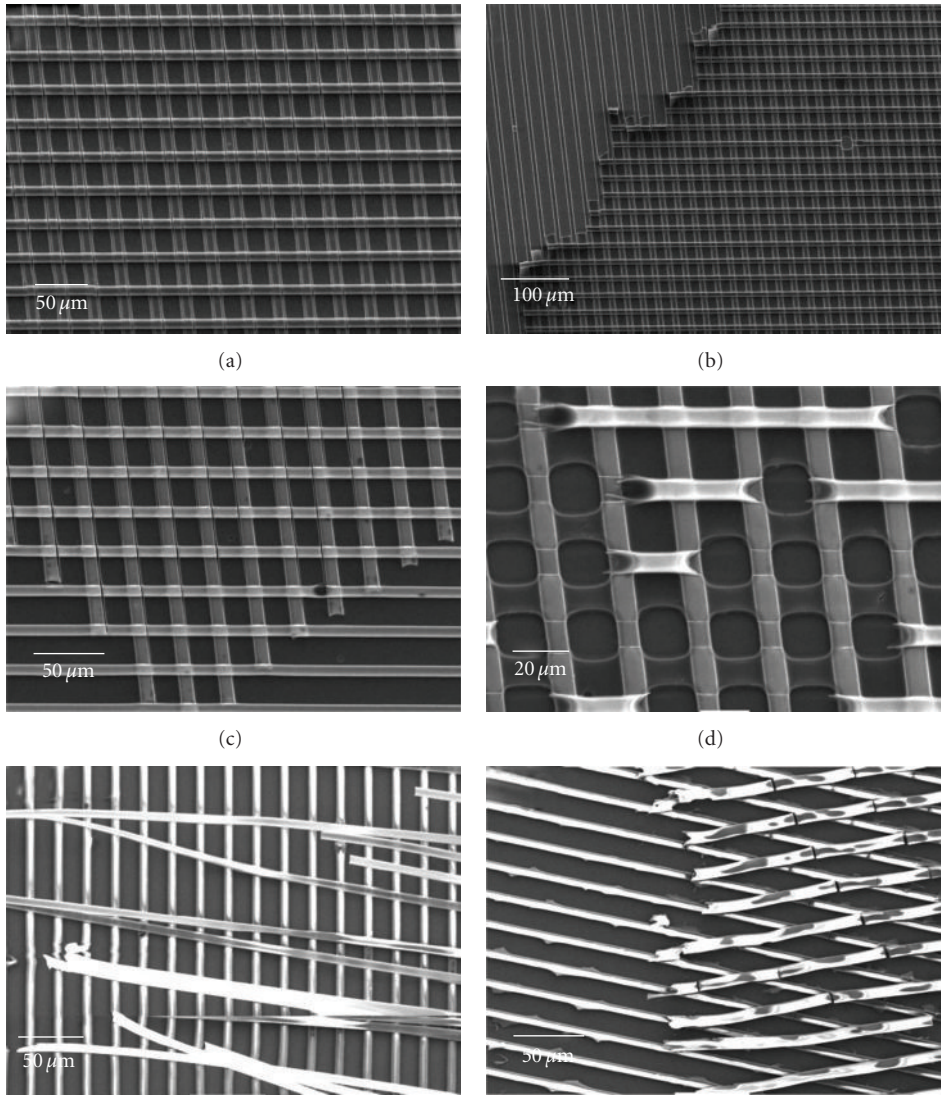

Figure 6: SEM images of 3D patterns. (a) μTM-derived dual layer pattern; (b) detached second layer of a pattern showing the residue layer; (c) 3D pattern showing cracks at the point of contact; (d) effect of incomplete drying of the second layer on pattern coherence and adhesion; (e) dual layer pattern where first layer was made with MIMIC and second layer with μTM; (f) μTM-derived dual layer patterns. The lines are at ca. 120° with respect to the others. Fractures are visible at the points of contact.

patterning is targeted. Formation of a residue layer is another limitation of MIMIC, even though absence of residue layers was one of the underlying reasons to develop MIMIC in the first place. These two problems were avoided by using μTM for 3D patterning.

Figure 6(a) shows μTM-made 3D pattern having a w_l of 6 μm derived of hybrid organosilica-embedded $LaPO_4$: Eu NPs. Care must be taken to remove the excess solution before bringing it onto the substrate. Otherwise, some residue layer will stay on top of the first layer; this undesirable layer can be seen in Figure 6(b) near the area of detachment of the second layer. Prior to the deposition of the second layer in μTM, the wet solution in the channels should be dried for a period of time, that is, partially gelled. Otherwise, it may penetrate into the underlying layer and result in defected pattern (Figures 6(c) and 6(d)). This should be done before the solution bond to the mould channels, since in that case it might not transfer to the substrate. The time period may vary for different materials and solvents; however, in the present scenario a time interval of 2-3 min was found to be the optimum.

The adhesion of the μTM-derived second layer to the underlying layer was found to be weak as compared to those derived from MIMIC. Eventually, this leads to detachment of the top layer, as illustrated in Figure 6(e). The second layer was also deposited under other angles to see if that might improve the adhesion of the second layer, but this also resulted in cracked lines (Figure 6(f)). The cracking of lines probably result from stresses that occur due to shrinkage of the second layer when the pattern dries.

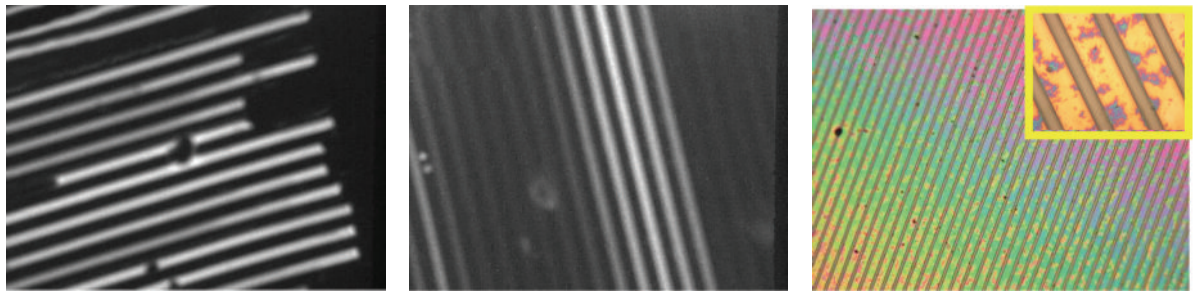

(a) (b) (c)

Figure 7: (a) and (b) Photoluminescence micrographs of $LaPO_4$: Eu line patterns with $w_l = 4\,\mu$m, excited with 260 nm UV light, showing reduced luminescence intensity; (c) optical micrograph of a $CePO_4$: Tb patterned film with $w_l = 6\,\mu$m, depicting residues and color contrast due to thickness variations of a few nanometers.

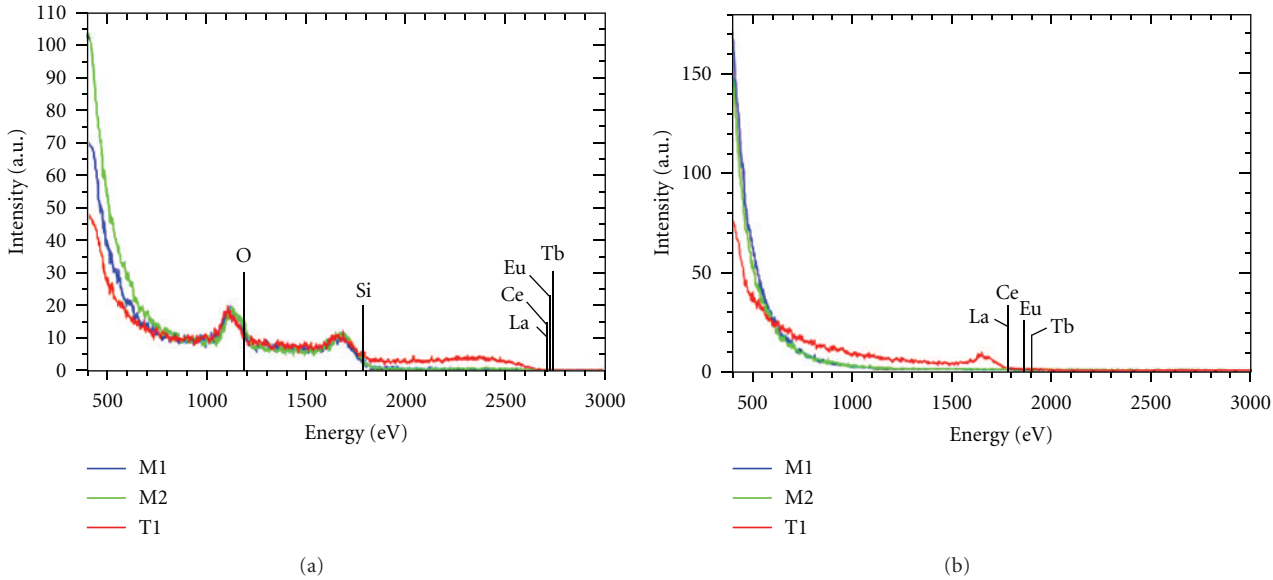

Figure 8: LEIS spectra of (a) He and (b) Ne scattering of $LaPO_4$: Eu NPs (M1) patterned by MIMIC; $CePO_4$: Tb NPs (M2) patterned by MIMIC; $LaPO_4$: Eu NPs (T1) patterned by μTM. All lines were made with same mould having $w_l = 6\,\mu$m, and NPs were embedded in hybrid organosilica.

3.6. Photoluminescence Microscopy. Eu has maximum luminescence (fluorescence) at $\lambda = 393$ nm, whereas for $LaPO_4$: Eu the best excitation is at 260 nm [1–5]. Figures 7(a) and 7(b) show the photoluminescence (fluorescence) micrographs of a $LaPO_4$: Eu patterned film made with MIMIC. These patterned films were studied with optical microscopy using an excitation wavelength of 260–300 nm. The photoluminescence intensity, however, was very low as can be seen in the figure. X-ray photoelectron spectroscopy (XPS) was performed to study the presence of the NPs in the patterned films. However, the results (not presented here) did not show indications for the presence of NPs in the patterned lines. The following possible reasons can be sum up about the reduced luminescence intensities.

Firstly, that the NPs are not present in the upper layers of the patterned lines, since XPS can give information up to 20 Å with an exponential decay towards the depth. The sensitivity of XPS is limited to 0.1–0.2 at%, depending on material. Lower concentrations will not be detected.

Furthermore, the microscope lenses were made from glass, which absorbs UV light. Thus, the microscope itself may have reduced the observed intensity drastically. A mercury lamp ($\lambda = 254$ nm) was also tried, but the intensity remained low. The excitation and emission wavelengths may also be affected by the matrix material. The hybrid organosilica matrix may reduce the optical yield by several orders of magnitude. Other reasons might include quenching effects such as phonon emission, where the energy of the excited state is consumed in the form of vibrational energy. Nevertheless, a detailed investigation into this effect was not within the scope of this research work. Figure 7(c) shows optical micrograph of a MIMIC-patterned film of $CePO_4$: Tb. The color spectrum indicates the presence of a residue layer, and the color contrast is indicative of thickness variation. The dark spots are small dust particles.

3.7. Low Energy Ion Scattering Analysis. To look in more detail to the surface composition than is possible with XPS,

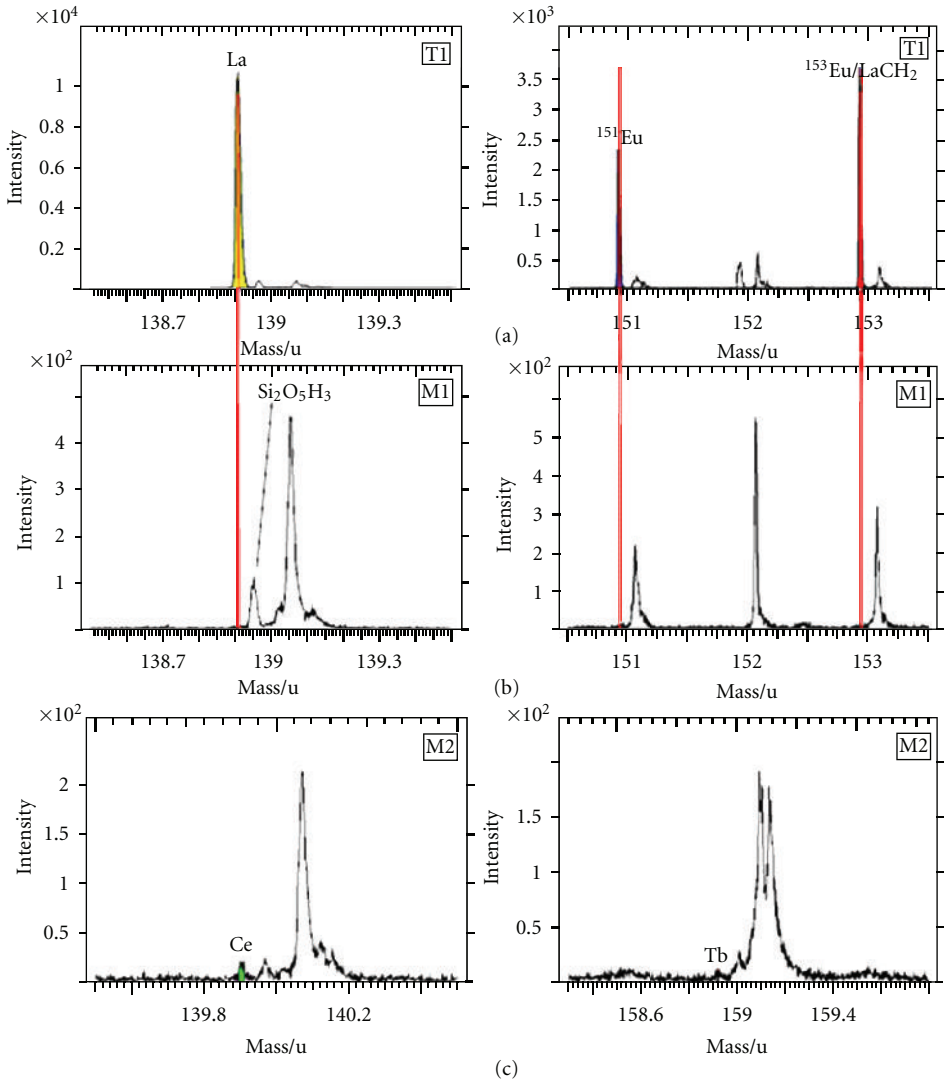

Figure 9: TOF-SIMS spectra of (a) T1 ($LaPO_4$: Eu NPs lines by μTM); (b) M1 ($LaPO_4$: Eu NPs patterned by MIMIC); (c) M2 ($CePO_4$: Tb NPs patterned by MIMIC).

compositional analyses of other three representative samples were done with the low energy ion scattering (LEIS) technique. LEIS can register lower element concentrations, but only in the upper atomic layer. One of the samples (M1), shown in Figure 1(a), is a MIMIC-derived line patterned film of $LaPO_4$: Eu NPs. The second sample (M2) is shown in Figure 3(a) and is a MIMIC-made $CePO_4$: Tb-patterned film. The third sample (T1) is shown in Figure 2. It is a μTM-made $LaPO_4$: Eu-line patterned film. Henceforth, these samples will be represented by M1, M2, and T1, respectively.

LEIS was performed using helium for the identification of low mass elements, followed by neon scattering for the identification of high mass elements. This way the composition of the first atomic layer was studied by ion scattering. Figures 8(a) and 8(b) show the He and Ne LEIS spectra of the above three samples.

In samples M1 and M2, no rare earth elements were detected. A likely reason is that the concentration of NPs is below the detection limit, at least in the top most layers. Since LEIS is sensitive only to the top atomic layer and cannot detect elements below a few atomic layers. On the other hand, Sample T1 showed the presence of lanthanum (La) in the outermost monolayer. The difference between the samples lies only in the use of the applied patterning technique, which suggests that the NPs are not present in the upper top layer of MIMIC-derived samples. Major differences resulting from the two soft-lithographic techniques are related to differences in filling behavior and differences in evaporation rates of solvent, and so forth. These may affect the concentration of NPs in the upper most regions of the patterned lines.

3.8. Secondary Ion Mass Spectroscopy Analysis. Time of flight (TOF) secondary ion mass spectroscopy (SIMS) was performed on the same samples as mentioned in the above section.

In all three samples, clear signs of SiOH compounds were detected. Sample T1 showed the presence of La and Eu along with the phosphates (Figure 9(a)). However, for sample M1

neither La nor Eu could be detected (Figure 9(b)). Similarly, for sample M2, a limited amount of Ce and Tb was detected (Figure 9(c)). Furthermore, no phosphates were found in the two samples (Figures 9(b) and 9(c)). Aliphatic and aromatic hydrocarbons were detected in these two samples. The aromatic compounds probably may have resulted from the initial synthesis of the NPs and, therefore, indirectly suggests their presence in the materials under investigation here.

On the basis of compositional analysis with LEIS and SIMS, some indications for the reasons for the reduced intensities observed with PL microscopy can be deduced. Firstly, the NPs are not near to the surface region. The path that photons have to travel to escape from the organosilica matrix is therefore relatively long; this affects the degree of absorption by the organosilica matrix. Furthermore, the sample patterned with μTM showed the presence of NPs very near to the external surface. This suggests that the patterning technique also has an influence on the location of NPs in the matrix material in the given pattern. Silica is known to be a good host material for lanthanide ions such as europium and cerium; however, quenching effects may reduce the photoluminescence intensity.

4. Conclusions

MIMIC and μTM techniques were applied successfully to pattern $LaPO_4$: Eu and $CePO_4$: Tb NPs embedded in hybrid silica. The shape of the patterned lines derived from MIMIC was found to be different from those derived with μTM. The adhesion of the patterned material to the substrate and to the mould was very challenging, and further work is needed to be done for a variety of other materials system to be able to reproduce the results. Furthermore, the adhesion of MIMIC-derived patterns to the substrate and the underlying pattern was stronger than that of μTM-made patterns. This is probably due to the fact that the residue layer in MIMIC is thicker, which improves bonding to the substrate. Also, in MIMIC the bonding is stronger due to the fact that in μTM the sol is jellified (semi-dried) before it is transferred. On the other hand, the shape of patterns is better replicated with μTM than with MIMIC.

By comparison of the two techniques, it can be concluded that both techniques have their own advantages and limitations. The selection of an appropriate technique may depend on the applications of the patterned films. MIMIC is a good technique for applications where residue layer is not undesirable. Similarly, μTM is good for the patterning of isolated features and as well as when exact replication of the mould is desired.

Photoluminescence properties in the encapsulated NPs were studied. Their intensities were low. This may be either due to some quenching effects, and/or due to the fact that the NPs are buried away from the external surface. Other possibility could be that their amount is low. Nevertheless, the experiments show that both techniques can be used to pattern similar or other complex materials with these techniques.

Acknowledgments

Financial support from the Netherlands Technology Foundation STW within the framework of the VIDI Innovational Research Scheme is greatly acknowledged. The authors thank the Dutch Organization for Scientific Research (NWO) for the financial contribution to publish this work. They gratefully acknowledge Professor Karst and his group at the University of Münster for providing fluorescent nanoparticles and helping in the characterization of patterned films.

References

[1] H. Meyssamy, K. Riwotzki, A. Kornowski, S. Naused, and M. Haase, "Wet-chemical synthesis of doped colloidal nanomaterials: particles and fibers of $LaPO_4$:Eu, $LaPO_4$:Ce, and $LaPO_4$:Ce,Tb," *Advanced Materials*, vol. 11, no. 10, pp. 840–844, 1999.

[2] J. W. Stouwdam and F. C. J. M. van Veggel, "Near-infrared emission of redispersible Er^{3+}, Nd^{3+}, and Ho^{3+} doped LaF_3 nanoparticles," *Nano Letters*, vol. 2, no. 7, pp. 733–737, 2002.

[3] K. Riwotzki, H. Meyssamy, H. Schnablegger, A. Kornowski, and M. Haase, "Liquid-phase synthesis of colloids and redispersible powders of strongly luminescing $LaPO_4$:Ce,Tb nanocrystals," *Angewandte Chemie International Edition*, vol. 40, no. 3, pp. 573–576, 2001.

[4] W. Li and J. Lee, "Microwave-assisted sol-gel synthesis and photoluminescence characterization of $LaPO_4$:Eu^{3+},Li^+ nanophosphors," *Journal of Physical Chemistry C*, vol. 112, no. 31, pp. 11679–11684, 2008.

[5] J. W. Stouwdam, *Lanthanide-doped nanoparticles as the active optical medium in polymer-based devices*, Ph.D. thesis, University of Twente, 2004.

[6] E. Sluzky and K. Hesse, "Electrophoretic preparation of phosphor screens," *Journal of the Electrochemical Society*, vol. 136, pp. 2724–2727, 1989.

[7] J. B. Talbot, E. Sluzky, and S. K. Kurinec, "Electrophoretic deposition of monochrome and color phosphor screens for information displays," *Journal of Materials Science*, vol. 39, no. 3, pp. 771–778, 2004.

[8] M. A. Santana-Aranda and M. Meléndez-Lira, "Screen printed CdS_xTe_{1-x} films, structural and optical characterization," *Applied Surface Science*, vol. 175-176, pp. 538–542, 2001.

[9] M. B. Korzenski, P. Lecoeur, B. Mercey, and B. Raveau, "Nd:YVO_4 thin films grown by pulsed laser deposition: effects of temperature and pressure on the grain morphology and microstructure," *Chemistry of Materials*, vol. 13, no. 5, pp. 1545–1551, 2001.

[10] P. Lecoeur, M. B. Korzenski, A. Ambrosini, B. Mercey, P. Camy, and J. L. Doualan, "Growth of Er:Y_2O_3 thin films by pulsed laser ablation from metallic targets," *Applied Surface Science*, vol. 186, no. 1–4, pp. 403–407, 2002.

[11] E. W. Bohannan, X. Gao, K. R. Gaston, C. D. Doss, C. Sotiriou-Leventis, and N. Leventis, "Photolithographic patterning and doping of silica xerogel films," *Journal of Sol-Gel Science and Technology*, vol. 23, no. 3, pp. 235–245, 2002.

[12] M. Yu, J. Lin, Z. Wang et al., "Fabrication, patterning, and optical properties of nanocrystalline YVO_4:A (A = Eu^{3+}, Dy^{3+}, Sm^{3+}, Er^{3+}) phosphor films via sol-gel soft lithography," *Chemistry of Materials*, vol. 14, no. 5, pp. 2224–2231, 2002.

[13] Y. Xia and G. M. Whitesides, "Soft lithography," *Angewandte Chemie International Edition*, vol. 37, no. 5, pp. 550–575, 1998.

[14] D. Pisignano, M. F. Raganato, L. Persano et al., "The luminescence quantum yield of organic one-dimensional periodic nanostructures," *Nanotechnology*, vol. 15, no. 8, pp. 953–957, 2004.

[15] X. M. Han, J. Lin, J. Fu et al., "Fabrication, patterning and luminescence properties of X_2-Y_2SiO_5:A (A=Eu^{3+}, Tb^{3+}, Ce^{3+}) phosphor films via sol-gel soft lithography," *Solid State Sciences*, vol. 6, no. 4, pp. 349–355, 2004.

[16] E. Kim, Y. Xia, and G. M. Whitesides, "Micromolding in capillaries: applications in materials science," *Journal of the American Chemical Society*, vol. 118, no. 24, pp. 5722–5731, 1996.

[17] X. M. Zhao, Y. Xia, and G. M. Whitesides, "Fabrication of three-dimensional micro-structures: microtransfer molding," *Advanced Materials*, vol. 8, no. 10, pp. 837–840, 1996.

[18] K. Riwotzki, H. Meyssamy, A. Kornowski, and M. Haase, "Liquid-phase synthesis of doped nanoparticles: colloids of luminescing $LaPO_4$:Eu and $CePO_4$:Tb particles with a narrow particle size distribution," *Journal of Physical Chemistry B*, vol. 104, no. 13, pp. 2824–2828, 2000.

[19] S. U. Khan, O. F. Göbel, J. E. ten Elshof, and D. H. A. Blank, "Patterning lead zirconate titanate nanostructures at sub-200-nm resolution by soft confocal imprint lithography and nanotransfer molding," *ACS Applied Materials & Interfaces*, vol. 1, no. 10, pp. 2250–2255, 2009.

[20] C. R. Martin and I. A. Aksay, "Topographical evolution of lead zirconate titanate (PZT) thin films patterned by micromolding in capillaries," *Journal of Physical Chemistry B*, vol. 107, no. 18, pp. 4261–4268, 2003.